Hindawi
Geofluids
Volume 2022, Article ID 3064754, 16 pages
https://doi.org/10.1155/2022/3064754

Research Article

Temperature and Temperature Stress Analysis in Mass Concrete under Cold Environments of Strong Wind and Large Diurnal Temperature Range

Guoqing Wang,[1] **Meng He**,[1] **Canjun Zhou**,[1] **Wen Xie**,[1] **Xinglin Liu**,[1] **Jin Chen**,[1] **Hua Liu**,[1] **Bingbing Lei**,[2,3] **and Mingli Zhang**[2,3]

[1]*China Nuclear Industry Huachen Construction Engineering Co., Ltd., Xi'an, Shaanxi 712000, China*
[2]*School of Civil Engineering, Lanzhou University of Technology, Lanzhou, Gansu 730000, China*
[3]*Western Civil Engineering Research Center of Disaster Prevention and Mitigation, Ministry of Education, Lanzhou University of Technology, Lanzhou, Gansu 730050, China*

Correspondence should be addressed to Bingbing Lei; b_lei@foxmail.com

Received 11 November 2021; Accepted 21 April 2022; Published 16 May 2022

Academic Editor: Zhiwei Zhou

Special environmental condition with strong wind and large diurnal temperature range is not conducive for the control of crack development during the curing of mass concrete in the cold environment of Northwest China. In this study, the temperature at four measured points along the vertical profile of a mass concrete was measured over 14 days. Then, a thermal-mechanical model with the optimized initial condition, thermal parameters, boundary conditions, and the effects of rebar on temperature stress of concrete was built. Based on the observations and numerical model, the effects of environmental factor on the peak temperature, temperature fluctuation amplitude, and maximum temperature stress of the mass concrete are analyzed. The result showed that increasing wind speed can reduce the temperature of the concrete, but an opposite result is observed with increase in diurnal temperature range. Moreover, the more obvious diurnal variation of concrete temperature with the increase in wind speed and diurnal temperature range is not conducive to the thermal stability of the structure, especially for horizontal and side surfaces. Accordingly, increasing wind speed and diurnal temperature range will increase the peak temperature stress of the concrete and the overall stress level. Strong wind and large diurnal temperature range significantly increase the temperature stress and its duration for the side surface. The high temperature stress and intensive daily variation of temperature stress at the horizontal surface affect the durability of the concrete material. Therefore, the temperature stresses of the horizontal surface under wind speed levels 3, 4, 5, and 1.25 times large diurnal temperature range easily exceed the tensile strength; then, the temperature crack will appear. Combined with the research results, the temperature control and crack prevention measures are proposed under the condition of ensuring concrete strength. The study will further guide the improvement and optimization of mass concrete construction in an extreme environment.

1. Introduction

Under the interaction between the hydration heat and environment conditions, the cold shrinkage and thermal expansion of concrete promote the generation of cracks and seriously affect the structural durability of concrete [1, 2]. In particular, the mechanism of cement hydration is a very complex and interdependent chemical and physical process involved. Although the current state of knowledge on hydration is far from sufficient, there are generally accepted factors that affect the process [3–8]. From a construction process standpoint, environment variation is an important factor to be considered for temperature control during the placing and curing of mass concrete [2, 9, 10]. It is especially true for construction projects in the region of large diurnal temperature range (LDTR) and strong wind.

In the Northwest China, wind speed seriously affects the surface humidity characteristics and plays an important factor for the curing of mass concrete. The drying-shrinkage cracks appear to increase when environmental factors make the surface evaporation rate exceed the concrete bleeding rate [11–13]. Moreover, the effects of high air temperature, solar radiation, and low relative humidity may be more pronounced with increases in wind speed [14]. Field observations shows that the LDTR make the temperature of concrete be high enough to induce a substantial amount of evaporation in certain months as well [10, 15]. In the current construction practice, the humidity condition that allows the cement hydration process to proceed normally and proper surface curing measures, such as moisturizing curing method of plastic film in an early age, can reduce the drying-shrinkage of freshly placed concrete [10, 16, 17]. Moreover, the simple and accurate shrinkage equivalent temperature difference methods are adopted to consider the influence of drying-shrinkage cracks in this paper [18, 19].

The temperature cracks caused by LDTR and strong wind are a key problem for construction, even the different curing during the day and night [9, 20]. The temperature cracking due to thermal shrinkage is generally more severe in spring and autumn, when the daily and seasonal temperature differences are mostly obvious and the change of wind speed is various. In particular for mass concrete structures, it is a disadvantageous condition [14, 21]. The greater the temperature gradient between the surface and the interior of concrete caused by LDTR and strong wind, the greater the temperature stress and the more cracks are [22]. Moreover, according to Fourier's law of thermal conduction, the time rate of heat transfer through a material is proportional to the negative temperature gradient and the area, at right angles to that gradient, through which the heat flows [23]. Under LDTR and strong wind, the heat transfer process will fluctuate widely to bring uncertainty on temperature control for mass concrete during the concrete placing and curing. Concrete exposed to rapid heating or cooling condition has a lower tensile strain capacity and is more susceptible to shrinking and cracking [1]. Therefore, in the whole process of concrete placing and curing, it is necessary to study the influence of short-term significant changes of LDTR and wind environment on the potential temperature stress and cracking in mass concrete.

Field temperature and stress testing are the most direct measures to obtain temperature and stress in the process of mass concrete curing, but its test cost is expensive, and the test steps are complex, which is not suitable for large-scale engineering applications [24, 25]. Numerical models are used to predict temperature cracks in the whole process of placing and curing which has been proven to be efficient and reliable. However, in the previous study, the simulation results deviate greatly from the measured results. The main reasons are that the difference in initial conditions, thermal parameters, and boundary characteristics was seriously ignored [2, 9, 26, 27]. As for the prediction of temperature stress, the constraint effect of rebars on temperature stress of concrete in the process of concrete hardening and the construction process, including rebar assembling, placing, and curing, are also important factors [28–30]. Therefore, it is necessary to consider some key factors affecting concrete temperature and temperature stress in the actual construction process. It will be beneficial to optimize the model and achieve the accuracy of guiding engineering construction.

In this study, taking a mass concrete project in a seasonally frozen soil area in Northwest China as an example, the concrete temperature and stress conditions under the action of LDTR and strong wind are analyzed. Basic concrete temperature data were monitored on site. Then, a thermal-mechanical model, combined with in situ observation data, was built to use the partial differential equations (PDEs) from finite element software, COMSOL MULTIPHYSICS. The effects of the optimized initial condition, thermal parameters, boundary conditions, and the rebar effect on temperature stress of concrete were considered in the model. Comparison of the measured concrete temperature data and the simulated results was performed to verify the feasibility of the model. Accordingly, the model is used to discuss the temperature change process and temperature stress level of mass concrete under the action of different grades of wind speed and LDTR. The results can provide reference for engineering.

2. Materials and Methods

The established model mainly considers the heat transfer process caused by concrete hydration heat and the temperature stress change process caused by temperature difference and drying shrinkage during concrete hardening. Moreover, several important factors, such as optimized initial condition, thermal parameters, boundary conditions, and the constraint effect of rebars on temperature stress of concrete, were also considered in the model. To facilitate the construction of mass concrete in cold regions and model optimization, we tested the temperature at different monitored points of mass concrete in the research site in the western end of Hexi Corridor; also, basic meteorological data was monitored.

Assumptions in model: (1) mass concrete structures are regarded as elastic materials; (2) consider the thermal conductivity characteristics of the concrete built-in rebars, and ignore its thermal expansion characteristics; (3) after the concrete is poured, the internal relative humidity is kept stable under standard curing conditions; (4) the foundation soil is continuous and isotropic; (5) ignore the influence of the unevenness of the mass concrete temperature distribution caused by the pouring sequence and time at the initial stage of the hydration heat; and (6) the constraint conditions of the same constraint surface are identical when calculating the temperature stress.

2.1. Mathematical Model

2.1.1. Heat Transfer. A temperature gradient is produced under the temperature difference between the concrete interior and the environment and the local temperature difference in the

concrete. For the temperature field, the heat exchange process of the concrete is considered as follows [23, 31]:

$$\rho \cdot C_p \frac{\partial T}{\partial t} + \nabla \cdot (-k \cdot \nabla T) = Q + Q_{\text{ted}}, \tag{1}$$

where t is the time (s), ρ is the concrete density (kg m^{-3}), T is the concrete temperature (°C), C_p is the heat capacity of the reinforced concrete (kJ kg^{-1}°C^{-1}), and k is the heat conductivity (kJ m^{-1}s^{-1}°C^{-1}). Q_{ted} is the elastic damped heat (kJ), which is ignored in the study. The factors that can affect the thermal properties of the concrete include the amount and thermal properties of the aggregate, temperature, and water content of the concrete. They should be determined by using the weighted average method [19].

$$\begin{aligned} C_p &= \frac{\sum C_i \cdot W_i}{W_{\text{G}}}, \\ k &= \frac{\sum k_i \cdot W_i}{W_{\text{G}}}, \end{aligned} \tag{2}$$

where C_i (kJ kg^{-1}°C^{-1}), k_i (kJ m^{-1}s^{-1}°C^{-1}), and W_i (kg) are the heat capacity, heat conductivity, and weight of each ingredient of the reinforced concrete, respectively, and W_{G} is the gross weight (kg).

The rate of hydration heat, Q, is the hydration heat generated by a unit volume of concrete in a unit time (W m^3), which continuously decreases with the hydration process of the mass concrete [31, 32].

$$\begin{aligned} Q &= \frac{W}{C_\rho \cdot \rho} \cdot \frac{dQ_t}{dt}, \\ Q_t &= Q_c\left(1 - e^{-m \cdot t}\right), \end{aligned} \tag{3}$$

where W is the amount of cementing material of concrete. Q_t is the hydration heat with age (kJ), which can be estimated from the hydration heat values after 7-day and 3-day age [2, 33]. m is the hydration coefficient. The total hydration heat of the cementitious material, Q_c (kJ), was considered under the effect of different cement admixtures.

2.1.2. Temperature Stress Change. The change in the concrete mechanic's characteristics with time during the process of hydration hardening is a key for influencing the concrete performance. In the theory of concrete structure, a simplified calculation model is proposed, which assumes that the concrete aggregate is circular, does not deform, and is uniformly distributed in the homogeneous elastic cement [19]. The corresponding equation is as follows:

$$\rho \frac{\partial^2 u}{\partial t^2} = \nabla \cdot (C : (-\xi_{\text{th}})) + f, \tag{4}$$

where u is the displacement of the concrete (m). $C(E, \mu)$ is the constitutive parameter tensor related to the elastic modulus, μ is Poisson's ratio of concrete, and E is the concrete elastic modulus (N m^{-2}). f is the volume load (N m^{-3}), and ξ_{th} is the concrete strain due to the temperature change (m m^{-1}).

The elastic modulus of the cement is constantly changing during the hydration process [34, 35]. As the age increases, the growth rate decreases, and the elastic modulus tends to be constant after the final hydration process [36]. Its change over time can be characterized by a negative exponential function:

$$E(t) = \beta \cdot E_0\left(1 - e^{-\varphi \cdot t}\right), \tag{5}$$

where β is the correction coefficient of the concrete elastic modulus with admixtures and $\beta = \beta_1 \cdot \beta_2$. E_0 is the concrete elastic modulus after 28-day age under the standard curing condition (N m^{-2}), and φ is an empirical coefficient.

In the temperature change process of mass concrete structure, the shrinkage and expansion will be limited [37], resulting in the self-confining temperature stress and the external confining temperature stress. Therefore, temperature stress is considered as

$$\sigma_Z(t) = \frac{a}{2} \times \Delta T_1(t) \times E(t) \times K(t, \tau), \tag{6}$$

$$\sigma_X(t) = \frac{a}{1 - \mu} \times \Delta T_2(t) \times E(t) \times R(t) \times K(t, \tau), \tag{7}$$

$$R(t) = 1 - \left(\frac{1}{\cosh\left(\sqrt{C_X/(H \cdot E(t))} \cdot L/2\right)}\right), \tag{8}$$

where a is the linear expansion coefficient of the concrete (°C^{-1}). $\Delta T_1(t)$ is the temperature difference between the center and the surface of concrete (°C), $K(t, \tau)$ is the stress relaxation coefficient of the concrete, t is the stress-generated time (s), and τ is the stress-held time (s). $\Delta T_2(t)$ is the comprehensive temperature difference reduction of concrete. $R(t)$ is a generalized constraint coefficient, where C_X is the horizontal deformation stiffness of the external constraint (N m^{-3}) [19, 33], H is the concrete structure thickness (m), and L is the length of the concrete deposit (m).

$\Delta T_S(t)$, a shrinkage equivalent temperature difference, is introduced to quantitatively study the concrete shrinkage (°C) [18, 33]. The concrete dry shrinkage becomes equivalent to the temperature shrinkage effect as the temperature decreases. The temperature difference index mentioned above is expressed as follows:

$$\Delta T_S(t) = -\frac{\left[\xi_y^0\left(1 - e^{-0.01 \times t}\right) \times \prod_{i=1}^{11} M_i\right]}{a}, \tag{9}$$

where ξ_y^0 is the final shrinkage deformation of the concrete under the standard test condition (m m^{-1}). M_i denotes the correction coefficients of the concrete shrinkage value under different conditions, which are listed in Table 1 [33].

To avoid the crack occurring under the temperature difference at the curing age of concrete, the concrete internal

Table 1: Correction coefficient.

Coefficient	M_1	M_2	M_3	M_4	M_5	M_6	M_7	M_8	M_9	M_{10}	M_{11}
Value	1.0	1.13	0.98	1.66	1.09	0.70	0.65	0.61	1.30	0.87	1.01

and surface stresses should not exceed the standard value of the tensile strength [38, 39]:

$$\begin{aligned} \sigma_Z(t) &\le \frac{f_{tk}(t)}{K}, \\ \sigma_X(t) &\le \frac{f_{tk}(t)}{K}, \\ f_{tk}(t) &= f_{tk}\left(1 - e^{-\gamma \cdot t}\right), \end{aligned} \tag{10}$$

where $f_{tk}(t)$ is the standard value of the tensile strength variation with age ($\mathrm{N\,m^{-2}}$), f_{tk} is the standard value of tensile strength ($\mathrm{N\,m^{-2}}$), γ is an empirical coefficient, and K is the safety factor of the crack resistance.

Due to the low reinforcement ratio of mass concrete, the thermal elastic deformation is mainly controlled by concrete [40]. The axial force of rebars was subjected to hydration heat expansion constraint of concrete [41]:

$$\rho_r \cdot A_r \cdot \frac{\partial^2 u_i}{\partial t^2} + \frac{\partial N_i}{\partial x_i} = f_i, \tag{11}$$

$$N_i = E_r \cdot \left(\frac{\partial u_i}{\partial x_i} - \xi_{\text{inel}}\right), \tag{12}$$

where A_r, ρ_r, and E_r are the cross-sectional area ($\mathrm{m^2}$), density ($\mathrm{kg\,m^{-3}}$), and elastic modulus of the rebars ($\mathrm{N\,m^{-2}}$, respectively. u_i, N_i, and f_i are the displacement (m), axial force (N), and body force ($\mathrm{N\,m^{-3}}$) in the x, y, and z directions, respectively. ξ_{inel} is the inelastic strain ($\mathrm{m\,m^{-1}}$).

2.1.3. Boundary Conditions. Based on Newton's cooling law, the normal heat flux at the boundary is related to the heat transfer coefficient, h, and the temperature difference of the internal and external concrete [2, 19, 26, 31]:

$$-n \cdot -k\nabla T = h(T_{\text{ext}} - T), \tag{13}$$

where T_{ext} is the ambient temperature (°C), when the effect of the wind speed, v ($\mathrm{m\,s^{-1}}$), is considered and the convective heat transfer coefficient ($\mathrm{W\,m^{-2}{}^{\circ}C^{-1}}$), h, is determined according to the test [33]. Therefore,

$$h = 5.46v + 6. \tag{14}$$

The heat release coefficient from the concrete surface to thermal insulation medium is considered [19, 31]

$$R_S = \frac{1}{h_{\text{ext}}} + \sum_i \frac{h_i}{\lambda_i}, \tag{15}$$

where R_S is the total thermal resistance of the insulation layers ($\mathrm{m^2{}^{\circ}C\,W^{-1}}$), h_{ext} is the heat transfer coefficient between the outermost material of insulation layers and air ($\mathrm{W\,m^{-2}{}^{\circ}C^{-1}}$), and h_i, λ_i are the thickness (m) and thermal conductivity of the insulation material ($\mathrm{kJ\,m^{-1}s^{-1}{}^{\circ}C^{-1}}$), respectively [19].

The boundary between the concrete structure and the foundation is considered poor contact. The affected factors, such as the air heat transfer coefficient and the radiant thermal conductivity of the contact void, are required to be considered [26, 31]. Moreover, there are two temperature indicators, the temperature of concrete, T (°C), and the temperature of foundation, T_f (°C).

$$k \cdot \frac{\partial T}{\partial t} = \frac{1}{R_C}(T_f - T), \tag{16}$$

$$k \cdot \frac{\partial T}{\partial t} = k_f \cdot \frac{\partial T_f}{\partial t}, \tag{17}$$

where R_C is the contact thermal resistance, which can be obtained from tests ($\mathrm{m^2{}^{\circ}C\,W^{-1}}$); k_f is the heat conductivity of foundation ($\mathrm{kJ\,m^{-1}s^{-1}{}^{\circ}C^{-1}}$). In this model, the boundary can be considered a constant heat flux [42].

The contact between the rebars and the concrete interface can be considered a good contact [19].

$$T = T_r, \tag{18}$$

$$k \cdot \frac{\partial T}{\partial t} = k_r \cdot \frac{\partial T_r}{\partial t}, \tag{19}$$

where T_r and k_r are the temperature (°C) and the heat conductivity of rebars ($\mathrm{kJ\,m^{-1}s^{-1}{}^{\circ}C^{-1}}$), respectively.

2.2. Model Implementation. The hydration heat causes the uneven distribution of temperature in mass concrete through the heat transfer and boundary heat exchange process, which will cause uneven expansion and temperature stress in concrete. The partial differential equation (PDE) model of COMSOL was used to solve the thermal-mechanical model. The governing equations (1), (4), and (11) are the key to building a numerical model. The relationship between the heat transfer process and the temperature stress change process is established by formulas (6)–(9) and (11)–(12). The model of multiphysical field interaction was built. In the whole process, the concrete and the rebar are assumed to be elastic deformation, and the development of mechanical parameters with the hydration process is considered. The PDE function of COMSOL is used to simulate the thermal state of foundation soil as well.

2.3. Field Observations

2.3.1. Study Site. The observation site is located at 39°47′N and 98°17′E in the western end of Hexi Corridor (Figure 1(a)). The

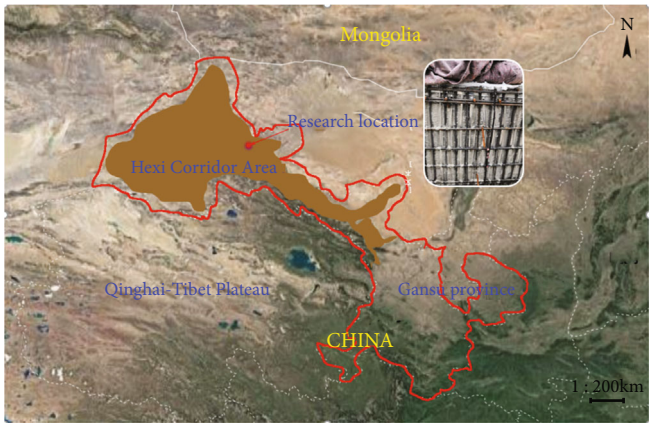

(a) Research location

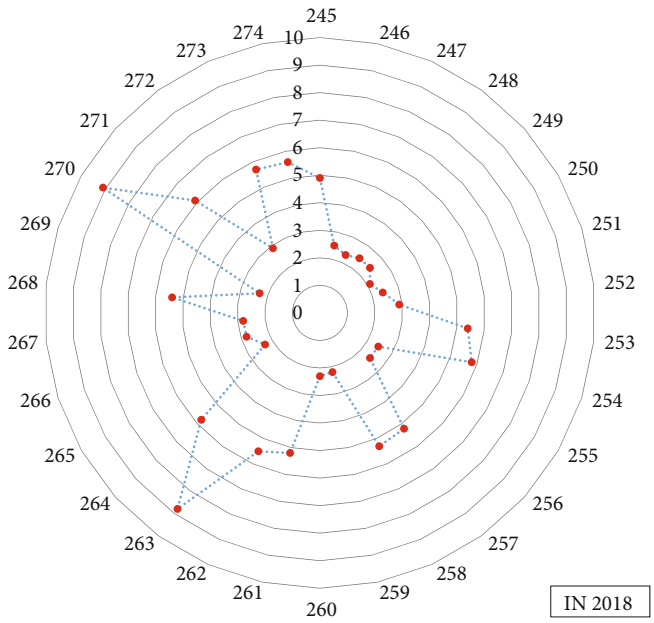

(b) Daily average wind speed

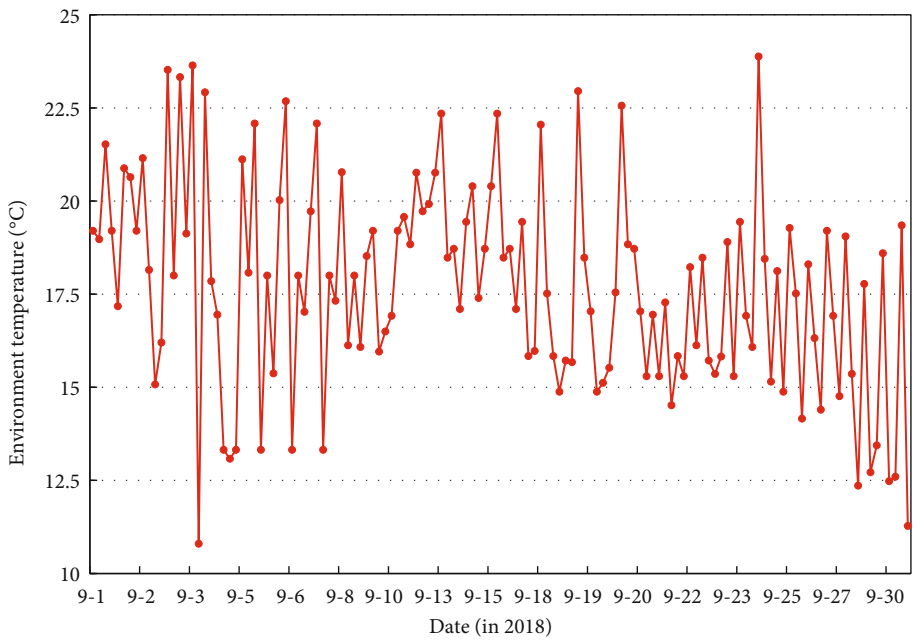

(c) Measured ambient temperature

Figure 1: Research location and environmental condition.

maximum wind speed at the natural site is 26 m s^{-1}, and the annual average wind speed is approximately 2.3 m s^{-1}. Under the influence of the air pressure of Eurasia and the terrain of Northwest China, strong wind weather is frequent (Figure 1(b)). There is a long sunshine duration, strong solar radiation, and maximum DTR that can reach above 23.4 °C, as shown in Figure 1(c). Basic information of mass concrete is shown in Table 2. The total pouring volume of the mass concrete is 1120.5 m^3, the pouring temperature is 25.6 °C, and the pouring time is up to 2 days by using layered inclined plane. According to the actual construction situation, the pouring date is October when LDTR and the northwest wind are prevailing. The surfaces of concrete were covered with a thin layer of plastic film to decrease evaporation. Besides the plastic film covering, a 20 mm thick layer of cotton covered the top of mass concrete to ensure thermal insulation under LDTR and strong wind weather. In order to facilitate the subsequent construction process, it was removed 3 days later. For the mass concrete structure, there were wooden formworks surrounding the four sides to act as both support and thermal insulation.

2.3.2. Observation Conditions. The placement of temperature sensors should be carried out after the process of built-in rebar binding in concrete (Figure 2). Four different-depth

Table 2: Basic information of mass concrete.

Information	Data	Information	Data
Concrete strength grade	C40	Rebar type	HRB400
Concrete mix ratio	$C : S : G : W = 1 : 2.36 : 3.53 : 0.48$	Water-binder ratio	0.38
Collapse degree	160 ± 30 mm	Reinforcement ratio	2.00%
S95 granulated blast furnace slag	10.21%	Fly ash	18.14%
HP-AE high-performance water reducer (kg)	6.00	Cement variety	P.O 42.5
Fineness of cement ($m^2\,kg^{-1}$)	400.00	Slurry volume	34.1%
Rs of cotton material $(K\,m^2\,W^{-1})$	0.32	*Rs* of wooden model $(K\,m^2\,W^{-1})$	0.20

C is cement, *S* is sand, *G* is gravel, and *W* is water.

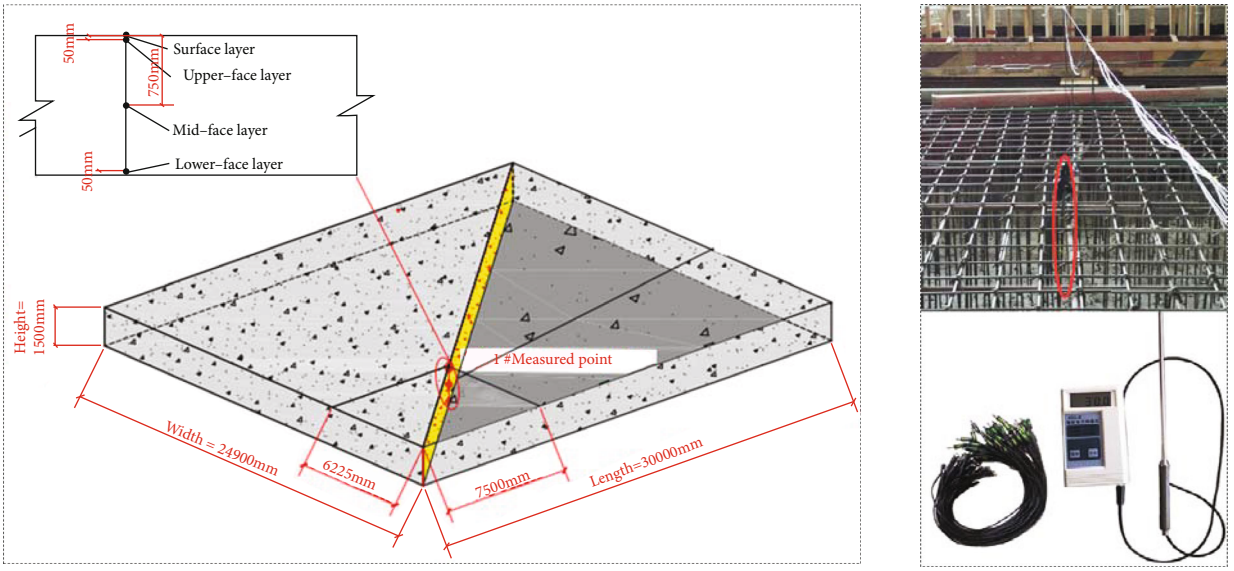

(a) Schematic diagram of monitored point location

(b) The real picture of the monitored point

Figure 2: Measured points in concrete structure (unit: mm).

measured points are selected on the same vertical profile of mass concrete. Three Pt1000 resistance temperature detector sensors (RTDS) were installed at 5 cm below the surface (upper-face layer), in the middle (midface layer), and above the bottom (lower-face layer), respectively. Apart from these RDTS, two thermometers were installed on the surface (surface layer) of concrete and in the air nearby to monitor the surface temperature of mass concrete and air temperature. Three Pt1000 and two thermometers have a range of −20~100 °C and measured the temperature with a resolution of 0.1 °C. During the monitoring, the Pt1000 sensors were bound on the rebar and separated with insulation tape to avoid direct contact with the rebar. Sensors were immersed in fresh concrete. All probes were connected to a data collector with a cable. Each data collector can send data wirelessly through an onboard 433 MHz transmitter module to the data host in a safer place.

2.4. Model Verification. A comparison of the measured and simulated results will be conducted to verify the accuracy and feasibility of the simulated temperature field. The synergistic effects between the hydration heat and the ambient temperature on the temperature stress and thermal cracks of the mass concrete are further researched. The simulation parameters are provided from basic data of mass concrete at the monitoring site and the standard for Construction of Mass Concrete (GB50496-2018), and all the parameters used in the solution of the numerical model are listed in Table 3.

The surfaces of mass concrete were covered with a thin layer of plastic film, which can be used for moisturizing curing in the early period (0 to 3 d). The curing materials of 20 mm cotton are placed on the horizontal upper surface of the concrete, and a wooden model at the side face. The rebars are placed 100 mm below the surface of the concrete (Figure 3). The boundary mainly includes the thermal boundary and the displacement boundary. The thermal insulation characteristics of the concrete surface cured material are determined by the second type of formulas (13) and (15). The contact boundary characteristics of mass concrete and foundation satisfy formulas (16) and (17). The boundary conditions of concrete and built-in rebars are explained by formulas (18) and (19). Except for the free boundary

Table 3: Parameters were used in the solution of the theoretical model.

Parameter	Value range	Value
ρ(kg m^{-3})	(2.44-2.50) ×10^{3}	2.44×10^{3}
k(kJ m^{-1} s^{-1} °C^{-1})	8.39-12.56	9.02
β_1(—)	0.95-1.00	0.99
β(—)	1.00-1.01	1.00
φ(—)	—	9.00×10^{-2}
$K(t,\tau)$	0.39-0.79	0.50
C_X(N m^{-3})	(1.00-1.50) ×10^{9}	1.50×10^{9}
L(m)	>1.00	3.00×10^{1}
f_{tk}(N m^{-2})	(1.78-2.64) ×10^{6}	2.39×10^{6}
K(—)	1.00-1.15	1.15
E_r(N m^{-2})	(2.00-2.10) ×10^{11}	2.00×10^{11}
h_i(m)	—	2.00×10^{-2}
k_f(kJ m^{-1} s^{-1} °C^{-1})	5.75-7.91	7.34
k_r(kJ m^{-1} s^{-1} °C^{-1})	(1.29-2.08) ×10^{2}	1.60×10^{2}
C_p(kJ kg^{-1} °C^{-1})	0.92-1.00	0.97
W(kg)	>3.30×10^{3}	3.44×10^{3}
m(—)	0.29-1.89	1.28
Q_c(kJ)	(1.52-6.76) ×10^{2}	3.72×10^{2}
β_2(—)	1.00-1.05	1.01
E_0(N m^{-2})	(2.80-3.45) ×10^{10}	3.25×10^{10}
a(°C^{-1})	(0.60-1.30) ×10^{-5}	1.00×10^{-5}
T_w(°C)	6.70-7.50	6.70
H(m)	>1.00	1.50
ξ_y^0(—)	(3.24-4.00) ×10^{-4}	3.24×10^{-4}
γ(—)	—	0.30
ρ_r(kg m^{-3})	—	7.85×10^{3}
A_r(m^2)	(1.13-10.17) ×10^{-4}	8.04×10^{-4}
R_C(m^2 °C W^{-1})	0.13-0.18	0.17

feature on the upper surface, the mechanical boundary of the mass concrete adopts the fixed boundary considering the generalized constraint coefficient formula (8). At the annual average geothermal depth, the temperature gradient is relatively constant and the lower boundary of the foundation model is 0.03 °C m^{-1} [43]. The initial temperature of the rebars was 25.6 °C, which was the same as the concrete. The temperature distribution along the depth of the foundation soil under the mass concrete was simulated by considering the phase change between ice and water, heat conduction, and heat transfer of water [44].

According to the shape and size of the research object and the research emphasis, the mesh should be subdivided. The linear rebars were refined into linear elements with a length of 0.25 m along the longitudinal direction. The concrete structure was subdivided into a mesh of 0.5 m × 0.5 m × 0.5 m. The grid of the foundation part is relatively moderate, and the maximum mesh is 1.0 m × 1.0 m × 1.0 m. The time step is a variable with the measured time. The initial time step is 3 h, and the maximum time step is 12 h. The mesh refinement and relative tolerance refinement are complementary. To ensure convergence and get an accurate calculating result, the allowable relative tolerance was 10^{-3}. The COMSOL MULTIPHYSICS detection function was used to obtain the maximum value in the calculation domain in real time. Therefore, the data analysis in Sections 2.4 and 3 shows the change in maximum values of temperature and stress on the horizontal surface and side face in the study.

As shown in Figure 4, the results fit well through the comparison between the simulated and measured temperatures, especially in deep positions (midface, lower-face layer). Due to the difference in the interaction strength between hydration heat and ambient temperature, the day-round amplitude of simulated temperature gradually faded with the depth increasing. The simulated value is slightly higher than the measured one (Figure 4(a)), especially in the early days. During the period of 3.5–8 d (day) after pouring, the simulated peak value is close to the measured one, with a difference of 1.4 °C. For the upper-face layer (Figure 4(b)), the measured peak temperature is 49.6 °C, and the time to peak is 2 d. The simulated peak value is 52.84 °C on 3 d. The time to measured peak is earlier than that of the simulated value. The reason is that the hydration heat loss of the transporting and pouring period was not considered in the verification model. For the midface layer, the fitting degree of temperature is higher than that of other temperature measuring points (Figure 4(c)). The time to the peak value of the hydration heat is close to the measured one, which is 2.5 d and 2.1 d, respectively. At the lower-face layer, the measured peak value is 52.80 °C on 4 d, and the simulated result reaches the peak of 52.92 °C on 4.5 d (Figure 4(d)). This is related to the temperature field and thermal characteristics of the foundation soil. In the 0–3 d early period, the measured value is also 2–6 °C higher than the simulation. It is owing to the heat storage in the bottom of the mass concrete occurring earlier than that in the upper part by the layered pouring in the actual condition. Overall, the simulation errors were acceptable, and the calculated results showed a good agreement with the measured data.

In the absence of measured results, the distribution and variation of temperature stress are needed for making predictions. Figure 5 shows the cloud image of the temperature stress distribution of mass concrete at different times. As the weak position of curing (double-sided heat dissipation), the corner of concrete is more vulnerable to environmental changes. The temperature stress of the surface edge and corner significantly increases in 1–3 d. The effect of curing materials and the temperature stress at other locations on the surface is small. As the concrete hooping effect, a phenomenon in which the ultimate tensile strength of concrete is significantly increased, inhibits the development of cracks on the lower edge of the concrete side face, the stress is small (Figure 6(a)). Briefly, the temperature stress of the horizontal face is larger and changes more rapidly than that of the side upper surface, and the temperature stress of the edge of the horizontal surface is larger and increases more rapidly than that of the surface center in the early period. Moreover, with the removal of the horizontal surface thermal insulation materials (3 days after pouring), the temperature stress of the horizontal surface starts to change from the edge to the interior and increases sharply. The change rule is similar to

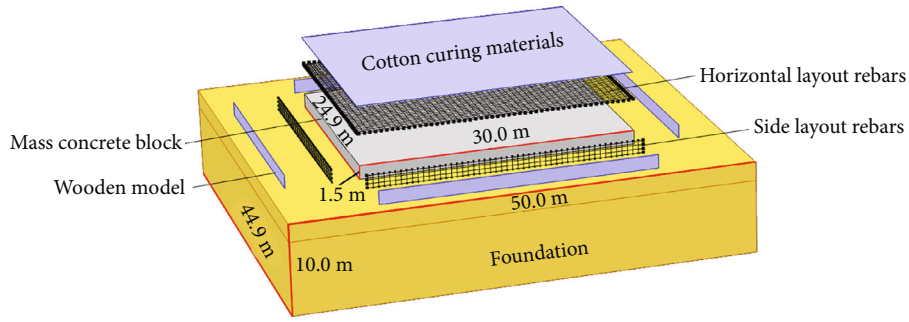

Figure 3: Geometry model of mass concrete.

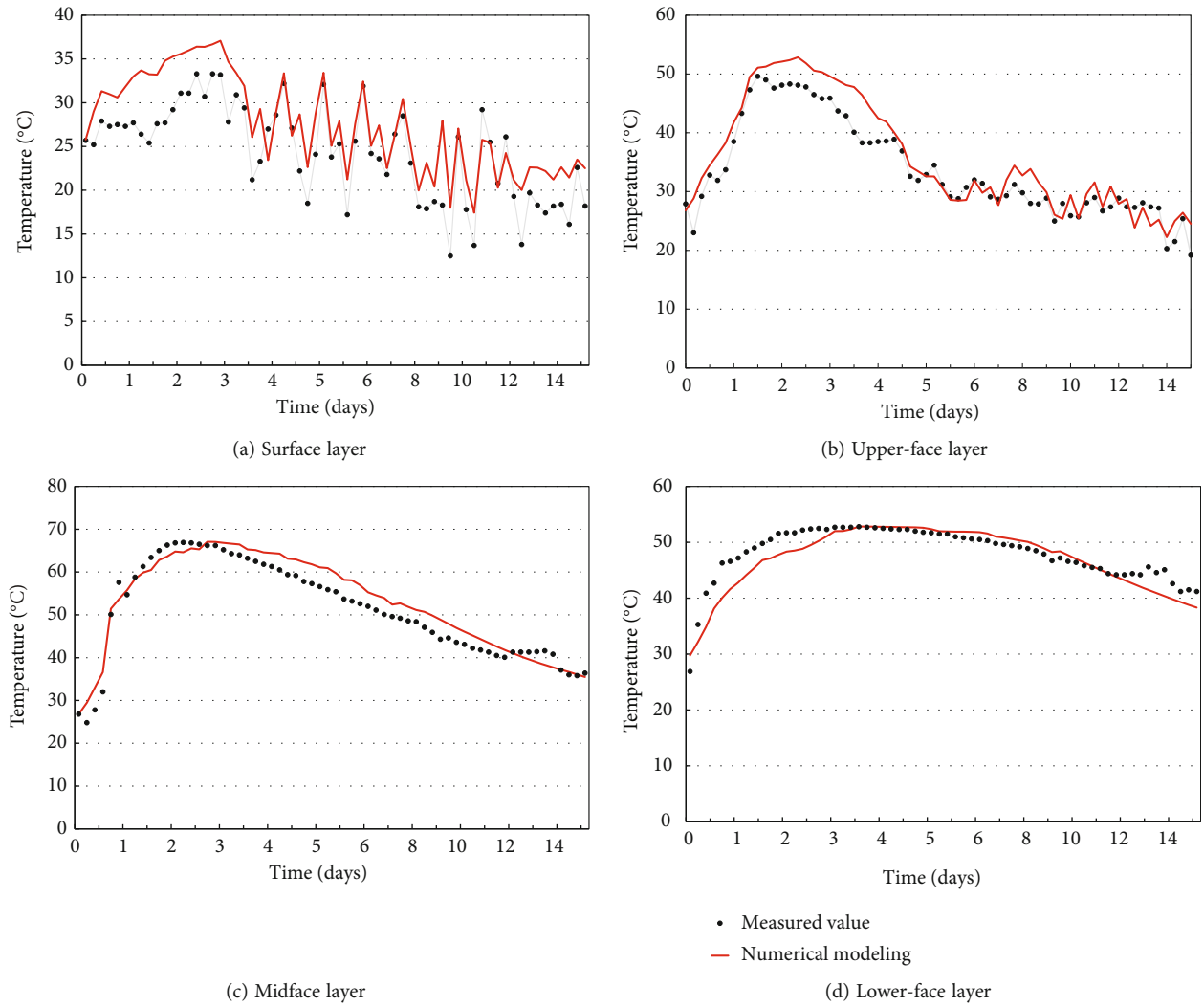

Figure 4: Measured and simulated results of temperature.

the empirical conclusion of concrete surface cracking summed up through a lot of engineering practice [2, 9, 19]. The maximum temperature stress change of different parts of concrete is shown in Figure 6(a). The axial stress of the upper rebars and lower rebars increases rapidly due to the dual effect of the environment (thermal characteristics of the foundation) and hydration heat (Figure 6(b)), while the stress of side rebars increases slowly due to the insulation and restraint of supporting materials. Therefore, it is feasible through the above mechanism analysis to predict the change of temperature stress in the period of curing.

2.5. Model Application. The good correlation between the measurements and simulated results is verified by the above numerical model. Based on the verification model, the boundary parameters are modified to study the variation in

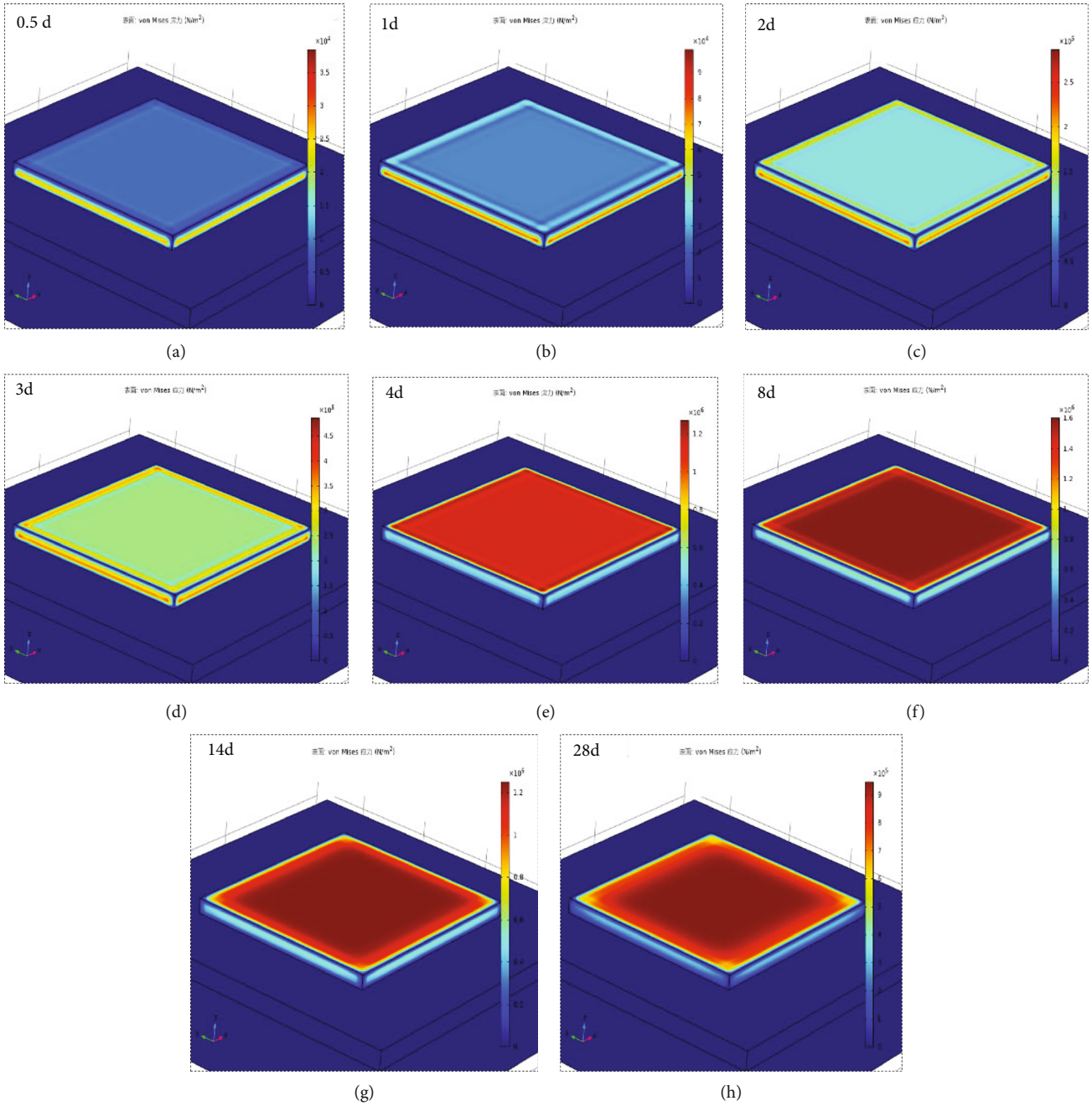

Figure 5: Temperature stresses in mass concrete at different ages.

the temperature and temperature stress in strong wind and large diurnal temperature range (LDTR) environments. According to the environmental condition of the study site, five conditions of wind speed (0 m s^{-1}, 2.5 m s^{-1}, 5.4 m s^{-1}, 7.9 m s^{-1}, and 10.7 m s^{-1}, i.e., 0 and 2 to 5 level winds) were used as the major wind speed conditions of the curing period to simulate. The thermal boundary condition at the ground surface used to study the LDTR case was calculated from formulas (13) and (14). Based on the original ambient temperature data of the curing period, the temperature and temperature stress field variations are simulated and analyzed when the diurnal temperature range is increased to 1.25 times LDTR (1.25 LDTR) and the DTR is decreased to 0.75 times LDTR (0.75 LDTR). The model parameters, geometry, mesh, and initial boundary conditions are the same as those of the verified model. Model establishment and solution are also based on COMSOL.

3. Results and Discussion

Based on the numerical model described above, the effects of each environmental factor (i.e., strong wind and large diurnal temperature range) on the peak temperature, temperature fluctuation amplitude, and maximum temperature stress of the mass concrete are analyzed using the variable-controlling approach.

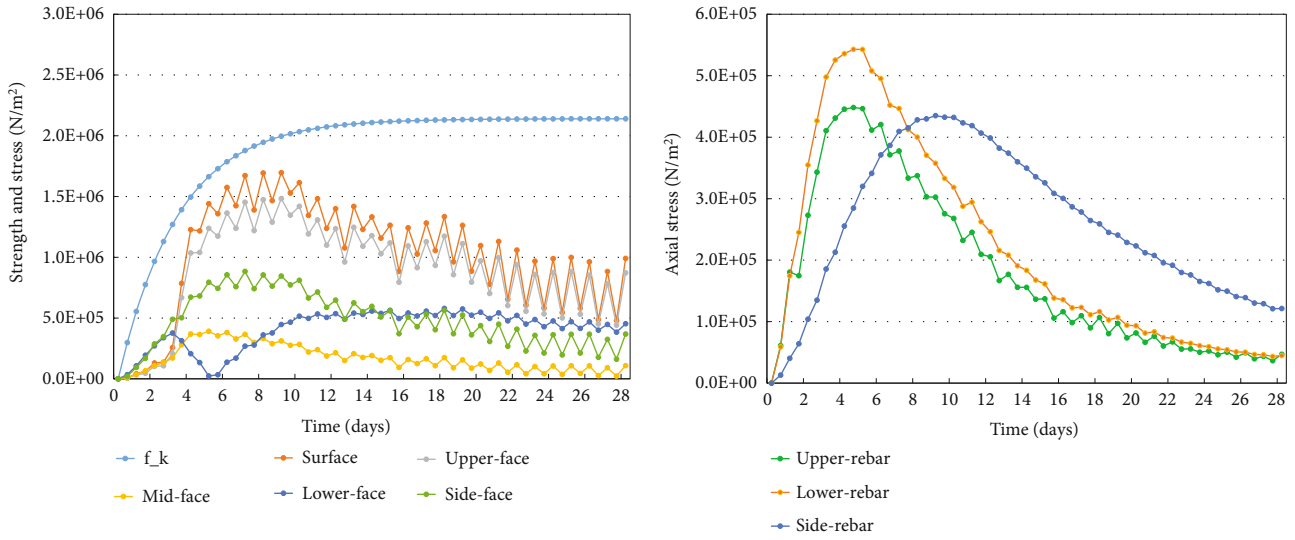

(a) Concrete (b) Rebars

Figure 6: Temperature stress and axial stress of rebar.

3.1. Strong Wind. Figure 7 shows the maximal temperature variation at different positions of mass concrete. The concrete temperatures increase obviously during the early curing period (0 to 3 days after pouring) but then decrease gradually. Figure 7(a) is the temperatures of the horizontal surface under different wind speeds. According to formulas (13) and (14), the increased wind speed increases the heat transfer coefficient of the concrete surface. It shows that the peak temperature on 3.5 d is 57.26 ˚C under the wind condition of 0 m/s. As the wind speed increases from level 2 to 5, the peak temperatures decrease to 38.48 ˚C, 32.98 ˚C, 31.06 ˚C, and 29.68 ˚C, respectively, and all the peak values occur at approximately 2.5 d. Because of the removal of curing materials 3 d after pouring, the maximal temperature fluctuation amplitudes are 2.03 ˚C, 4.92 ˚C, 5.93 ˚C, 5.96 ˚C, and 6.45 ˚C, respectively. For the concrete center, where the effect of hydration heat is stronger than that of strong wind, the peak temperature is 72.68 ˚C on 6.5 d under 0 m/s wind speed condition. On approximately 3.5 d, it decreases to 60.96 ˚C under wind level 2. The peaks decrease to 59.29 ˚C, 58.81 ˚C, and 58.47 ˚C under the conditions of wind levels 3, 4, and 5, respectively, and the time to peak is all 3 d (Figure 7(b)). Thus, there is no noticeable temperature fluctuation during the curing period. Regarding the side face (Figure 7(c)), the peak temperature on approximately 3.5 d is 54.76 ˚C under no-wind conditions. When the wind speed increased from level 2 to 5, the peak temperatures decrease to 47.93˚C, 47.34 ˚C, 47.16 ˚C, and 47.02 ˚C, respectively, and all the peak values occur at approximately 2.5 d. The maximal temperature fluctuations are 2.30 ˚C, 3.29 ˚C, 3.23 ˚C, 3.17 ˚C, and 4.15 ˚C, respectively, during 3.5–28 d after pouring. The temperature variation characteristics of side faces are different from the thermal characteristics of the horizontal surface, which is related to the difference in surface insulation materials and the difference in convective heat transfer coefficient between the vertical wall and the horizontal surface. From the above analysis, the influence of wind speed on the horizontal surface temperature of mass concrete is stronger than that on the side face and center. It is conducive to the cooling of concrete, but the obvious diurnal variation of concrete temperature with the increase in wind speed is not conducive to the thermal stability of the structure, particularly for horizontal and side surfaces.

Figure 8 shows the temperature stress changes of different parts of the concrete structure. In the early stage of the concrete curing, there is a definite increase in the temperature stress, following which under the condition of decreasing temperature difference, it reduces. Figure 8(a) is the temperatures stress of the horizontal surface under different wind speeds. It shows that the peak stress on 9.5 d is 0.76 MPa under the no-wind condition. As the wind speed rises from level 2 to 5, the peak temperature stress increases to 1.67 MPa, 1.85 MPa, 1.89 MPa, and 1.94 MPa, respectively, and the time to peak value after pouring is 9 d, 8 d, 8 d, and 8 d, respectively. Concurrently, the temperature stresses—1.47 MPa, 1.57 MPa, and 1.62 MPa—exceed the tensile strength of 1.43 MPa on the 4th day under wind levels 3, 4, and 5. Moreover, 4 to 10 days after pouring is the sensitive period of concrete surface cracking. It is mainly related to the strong influence of the environment and the constraints of surface rebars on the horizontal plane, primarily at the edges and corners of the horizontal surface. During the curing period, the temperature stress is induced by the action of temperature differences and self-weight. Due to symmetry, the temperature stress of the center is close to zero (Figure 8(b)). The peak temperature stresses are markedly smaller than the value of the tensile strength at this time. For the temperature stress of the side face (Figure 8(c)), all peaks are approximately 0.95 MPa in wind levels 0–4, and all the peak values occur at 7 d. However, due to strong boundary constraints, the peak value is 1.52 MPa in wind level 5 on

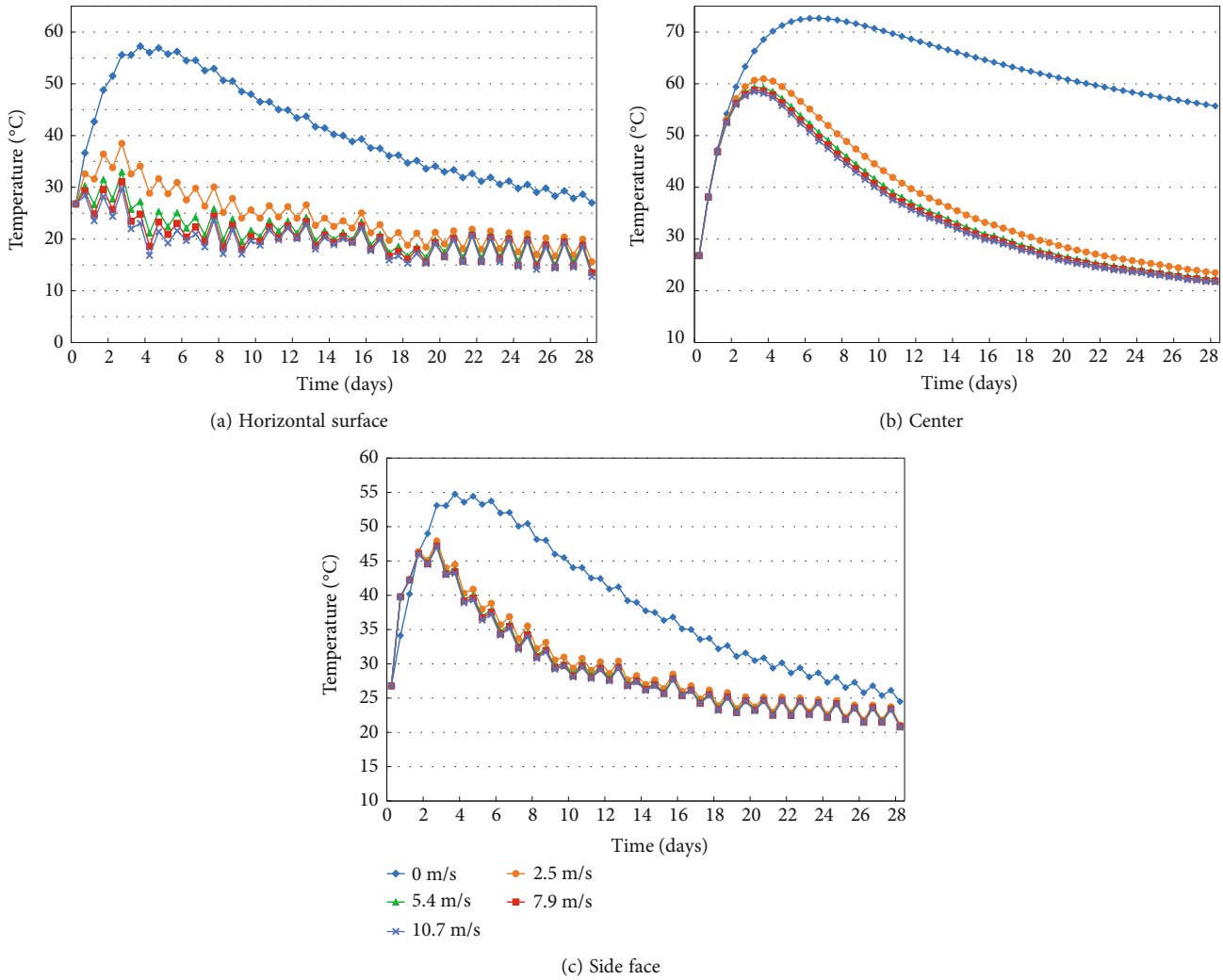

(a) Horizontal surface

(b) Center

(c) Side face

Figure 7: Maximal temperatures of concrete under different wind speeds.

19 d, and the reduction in temperature stress is also not remarkable after the time to peak. According to formulas (13) and (14), the increased wind speed increases the heat transfer coefficient of the concrete surface, which induces a significant temperature difference between the inside and outside of the concrete (Figures 7(a) and 7(b)). Therefore, the temperature stress will change significantly [14]. The influence of wind speed on horizontal surface temperature stress of mass concrete is stronger than that on the side surface and center. For the horizontal surface, strong wind speed may lead to the crack of concrete during the period to hydration heat peak. The intensive daily variation of temperature stress affects the durability of the concrete material. For the side surface, the increase in wind speed significantly increases the temperature stress and its duration.

Therefore, it is needed to adjust the curing conditions in time according to the variations of wind speed during the curing period. Engineering control measures not only ensure the temperature fluctuation amplitudes but also makes sure the temperature stress under the concrete strength. Some research results [2, 14, 19, 45] can be used to accomplish these engineering targets. In the windy conditions, adjusting the concrete pouring time based on basic environmental factors is vital to ensuring the quality of construction. The monitoring includes local weather and routine recording of conditions at the site, such as prevailing winds, air temperature, and relative humidity. These measured data provide reliable references for engineering supervisors to determine and prepare the required protective measures. Finally, curing materials should be available at the project site to adjust cooling and insulation measures in time, particularly at the edge and corner of mass concrete. Different types and thicknesses of curing materials are selected according to the velocity and duration of wind. For the curing of the side face, both temperature control and constraint conditions should be enhanced.

3.2. LDTR. In order to investigate the transfer process of the hydration heat and the temperature stress under large diurnal temperature range environments, the temperature and temperature stress variations are analyzed by the different diurnal temperature ranges of 1.25 LDTR, 1.0 LDTR, and 0.75 LDTR (Figures 9 and 10). During the

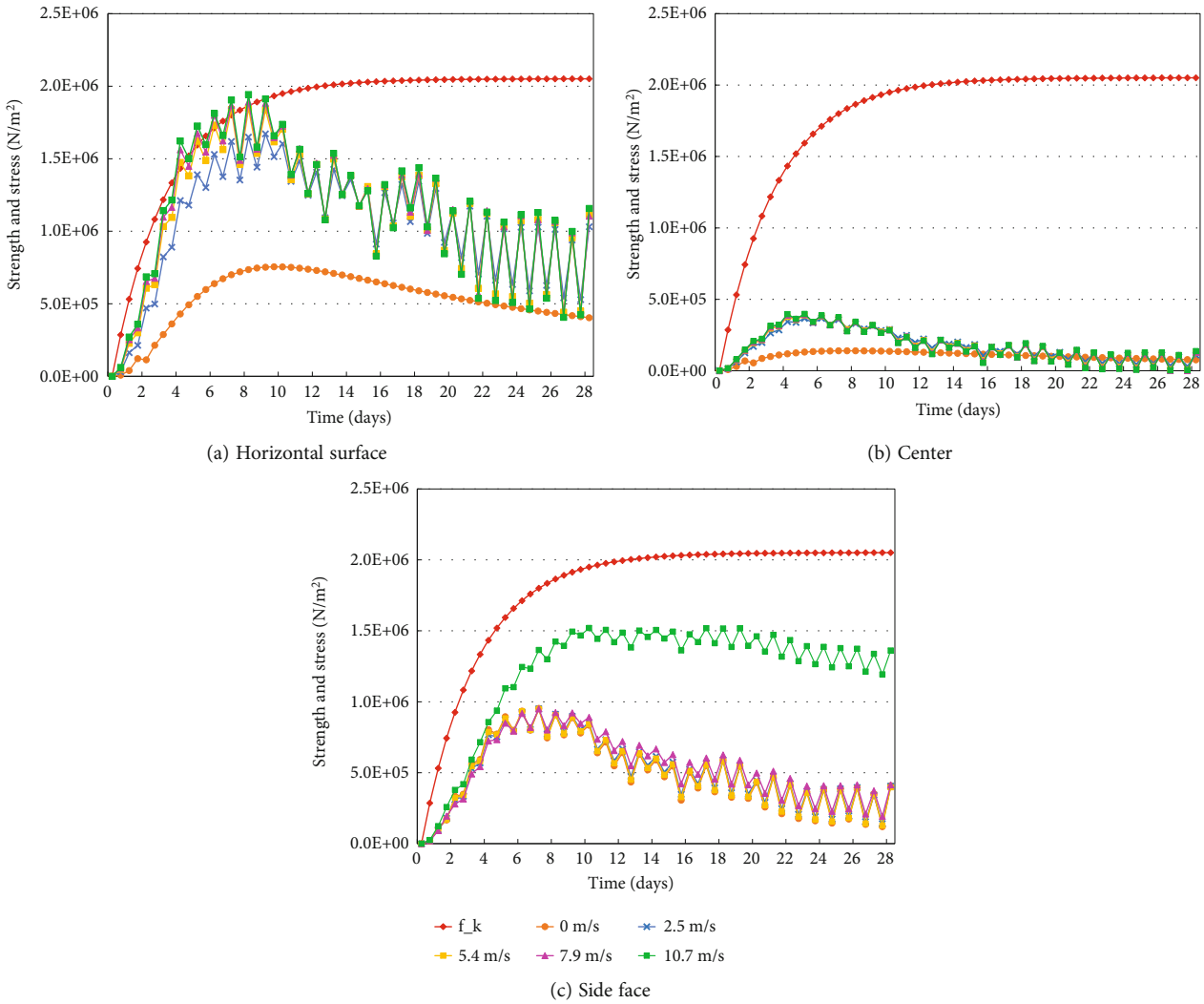

Figure 8: Maximum temperature stresses of concrete under different wind speeds.

0–3.5 d period when the heat of hydration is dominant, the increasing tendency of the concrete temperature is evident. And the mass concrete structure cooling is marked in the late period. Due to the influence of high ambient temperature during the daytime in LDTR, the peak temperatures of the horizontal surface under 0.75 LDTR, 1.0 LDTR, and 1.25 LDTR are 50.05 ˚C, 52.07 ˚C, and 54.83 ˚C, respectively, and all the peak values occur at approximately 2.5 d (Figure 9(a)). After the removal of the curing materials at the end of the third day, the maximum temperature fluctuation amplitudes are 4.09 ˚C, 6.30 ˚C, and 9.29 ˚C, respectively. For the center position, the effect of LDTR is weaken and there is no noticeable temperature fluctuation (Figure 9(b)). Regarding the side face (Figure 9(c)), the maximal temperature fluctuations are 2.41 ˚C, 3.47 ˚C, and 5.47 ˚C, respectively. It is different from the thermal characteristics of the horizontal surface, which is related to the difference in surface insulation materials and curing duration. From the above analysis, it can be obtained that the increase in the LDTR enhances the peak temperature and the effect of the LDTR on the temperature variation of the structure center is considerably smaller than that of the side face and the horizontal surface. Moreover, thermal shrinkage cracks are usually associated with a cooling rate of more than 3 $^{\circ}C\,h^{-1}$. The obvious diurnal variation of concrete temperature with the rise of LDTR is not conducive to the thermal stability of the structure, particularly for the horizontal surface and side face.

Figure 10 shows the temperature stress variations at different parts of the concrete structure. There is initially a definite increase in temperature stress, which is followed by a decrease. As for the horizontal surface (Figure 10(a)), from 0.75 LDTR to 1.25 LDTR, the peak temperature stresses are 1.53 MPa, 1.69 MPa, and 2.04 MPa, respectively, and all the peak values occur at approximately 8 d after pouring. The initial peak temperature stress is 1.75 MPa under 1.25 LDTR, which exceeds the tensile strength of 1.66 MPa. Moreover, 4.5–9 d is the sensitive period for concrete surface cracking under 1.25 LDTR. It is primarily related to the strong influence of the ambient temperature after the removal of the curing condition and the constraints of surface rebars on the horizontal surface. There is a clear increase in the temperature stress of the

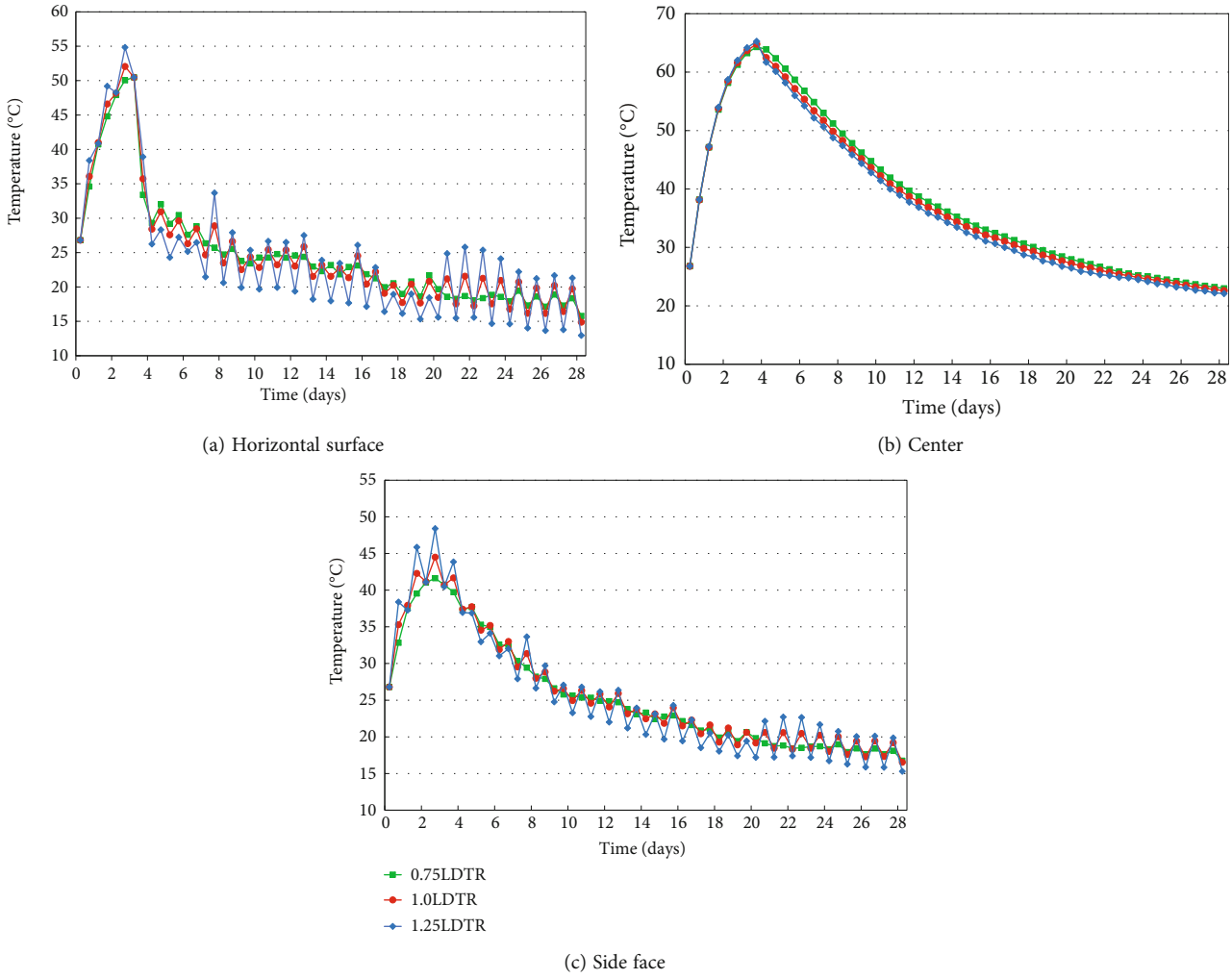

(a) Horizontal surface

(b) Center

(c) Side face

Figure 9: Maximum temperatures of concrete under different LDTRs.

surface during 3–4 d, and the growth of maximal temperature stress is 0.878 MPa, 0.963 MPa, and 1.181 MPa, respectively. The variations of temperature stress at the center under different LDTRs are small and the values are much smaller than the value of the tensile strength, which is similar to that of strong wind (Figure 10(b)). The peak temperature stresses of the side face are smaller than the instant tensile strength all the time (Figure 10(c)). In conclusion, the influence of LDTR on horizontal surface temperature stress of mass concrete is stronger than that of the side surface and center. With the increase in the LDTR, the stresses of the horizontal surface and the side surface remarkably increase by 37.6% and 35.8%, respectively. Horizontal surfaces are more prone to cracks than the side face under the action of the LDTR. In comparison, the temperature stress of the concrete center increases less, which is relatively stable.

Mass concrete is vulnerable to the influence of LDTR in the cold region, such as Northwest China. By observations and simulations, we found that the temperature variations of rise during the daytime and the sudden drop at night severely disturbed the temperature and thermal stress stability of its horizontal surface, center, and side face. In fact, the unreasonable control of the concrete construction in LDTR will affect the mechanical performance of the mass concrete and cause hidden problems for engineering [46]. By consideration of the construction schedule and the mass concrete quality, engineers need to control the maximum temperature stress to avoid structure cracking through some construction methods. Besides reducing the initial temperature of concrete, controlling the pouring time and pouring at night is advisable. Avoiding direct sunlight and strong solar radiation during the daytime is needed, which will reduce thermal shock from rapid temperature drops caused by LDTR or cool rain on concrete heated by the sunlight earlier in the day. Monitoring and predicting of local weather conditions, including air temperature, sun exposure, relative humidity, and prevailing winds, can be conducted locally. These data, together with projected or actual concrete temperatures, enable supervisors to precisely adjust the cooling measures by removing the curing mould during the daytime and to strengthen the heat preservation measures at night [1, 14, 47]. Based on the actual construction steps and key influencing factors, this paper predicts the temperature and temperature stress changes of the whole

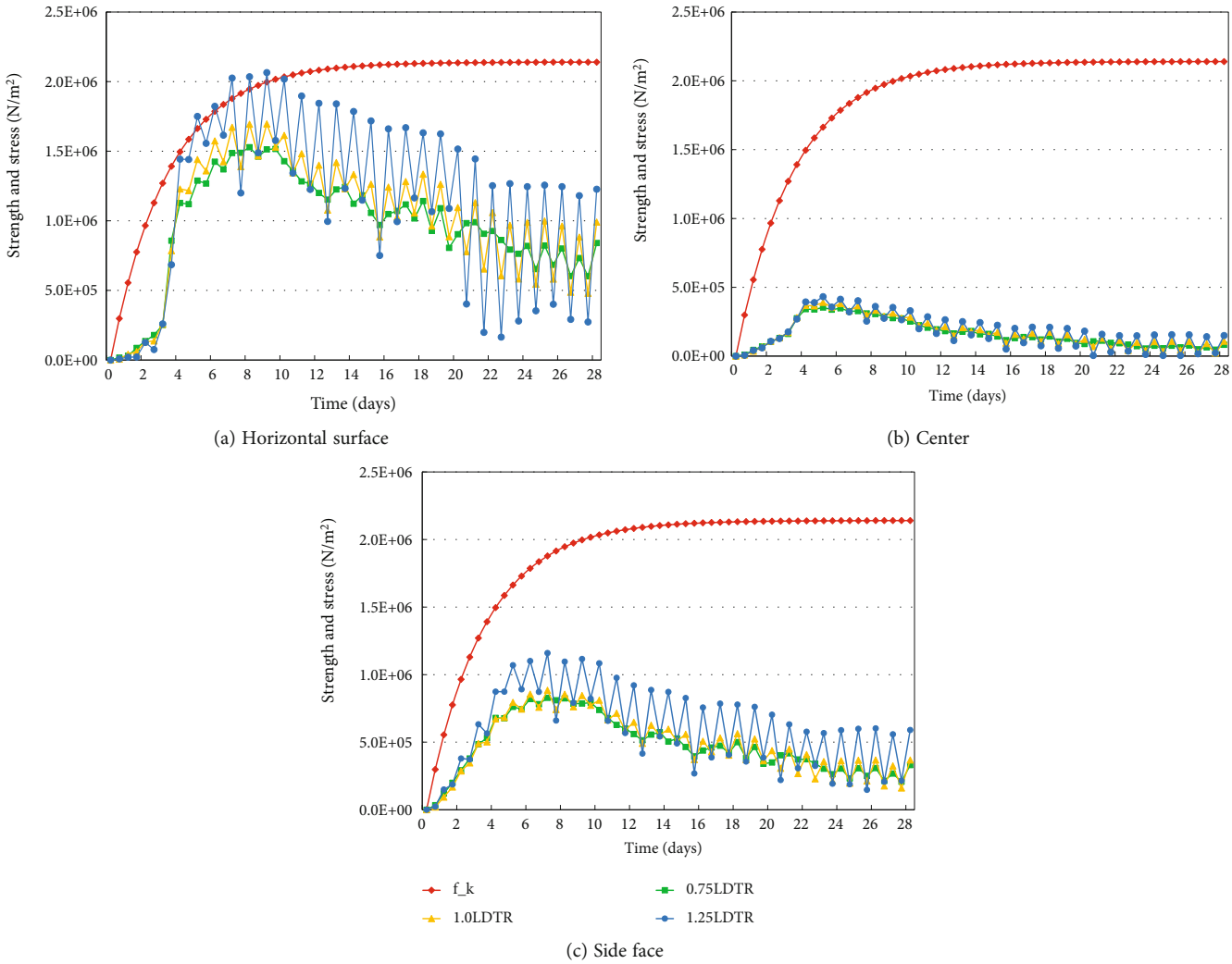

(a) Horizontal surface

(b) Center

(c) Side face

Figure 10: Maximum temperature stresses of concrete under different LDTRs.

curing process of mass concrete under the strong wind and LDTR in cold regions. It is useful to accurately evaluate the process of concrete cracking, as well as guide the improvement of the curing process of mass concrete in this area. However, there is insufficient research on the influence of moisture changes in newly poured concrete on the internal heat transfer process and temperature distribution.

4. Conclusion

Temperature and temperature stress analysis in mass concrete under cold environments of strong wind and large diurnal temperature range was performed. Some preliminary conclusions are drawn as follows:

(1) The increase in wind speed can reduce the temperature of the concrete but increase the peak temperature stress of the concrete and the overall stress level. The influences of wind speed on the horizontal surface temperature and temperature stress of mass concrete are stronger than those of the side face and center. Under the wind speed levels of 3, 4, and 5, the temperature stresses of the horizontal surface may exceed the tensile strength and lead to the crack of concrete during the period to hydration heat peak

(2) The increase in the diurnal temperature range (DTR) enhances the peak temperature and temperature stress

Moreover, the obvious diurnal variation of concrete temperature with the rise of DTR is not conducive to the thermal stability of the structure, particularly for the horizontal surface and side face. The influence of large diurnal temperature range (LDTR) on horizontal surface temperature stress of mass concrete is stronger than that of the side surface and center. With the increase in the DTR, the stresses of the horizontal surface and the side surface remarkably increase by 37.6% and 35.8%, respectively. Horizontal surfaces are more prone to cracks

than the side face and center under the action of the LDTR.

(3) In the windy conditions, adjusting the concrete pouring time based on basic environmental factors is vital to ensuring the quality of construction. And also, different types and thicknesses of curing materials are needed according to the velocity and duration of wind. Besides reducing the initial temperature of concrete, avoiding direct sunlight and strong solar radiation during the daytime is recommended. Monitoring and predicting of local weather conditions enable supervisor to determine and prepare the required protective measures

Data Availability

The data used to support the findings of this study are available from the corresponding author upon request.

Conflicts of Interest

The authors declare that they have no conflicts of interest.

References

[1] American Concrete Institute, *Report on Cooling and Insulating Systems for Mass Concrete (ACI 207.4R-20)*, American Concrete Institute, Michigan USA, 2020.

[2] B. F. Zhu, *Temperature Stress and Temperature Control of Mass Concrete*, China Water and Power Press, Beijing China, 2nd ed edition, 2012.

[3] K. A. Riding, J. L. Poole, K. J. Folliard, M. C. G. Juenger, and A. K. Schindler, "Modeling hydration of cementitious systems," *ACI Materials Journal*, vol. 109, no. 2, pp. 225–234, 2012.

[4] K. Meinhard and R. Lackner, "Multi-phase hydration model for prediction of hydration-heat release of blended cements," *Cement and Concrete Research*, vol. 38, no. 6, pp. 794–802, 2008.

[5] J. Gou, *Study on the Effect of Mass Concrete Hydration Heat on Structure*, Guangxi University, Nanning, 2008.

[6] D. W. Hou, J. Zhang, H. Y. Cheng, and W. Liu, "Development of strength and elastic modulus of concrete under moisture and drying curing conditions," *Journal of Hydraulic Engineering*, vol. 43, no. 2, pp. 198–208, 2012.

[7] J. Y. Wu, "Relation among raw materials, mix proportion, temperature rise and cracking performance of mass concrete," *Dam & Safety*, vol. 25, no. 2, pp. 28–31, 2011.

[8] J. Wang, *Study of Temperature Field and Temperature Stress Field in Mass Concrete of Raft Foundation*, Anhui Jian Zhu University, Hefei, 2015.

[9] Q. Shi, F. Q. Zhou, and Y. Wu, *Study and Practice of Temperature Field Variation Law of Mass Concrete in Cold Region (in Chinese)*, China Water and Power Press, Beijing China, 2010.

[10] Y. H. Hu, J. Chen, F. Zou et al., "A comparative study of temperature of mass concrete placed in August and November based on on-site measurement," *Case Studies in Construction Materials*, vol. 15, article e00694, 2021.

[11] P. J. Jiang and Q. C. Wang, "Influence of ambient humidity on compressive strength of concrete at constant low temperature," *Concrete*, vol. 41, no. 8, pp. 17–23, 2019.

[12] J. L. Si, Y. N. Qu, T. Yan, and Y. X. Wang, "Crack analysis and crack control of concrete buildings," *Construction & Design for Engineering*, vol. 69, no. 21, pp. 149–151, 2021.

[13] Y. Liu, *Internal Humidity Migration of Concrete Environmental Humidity Influence on Mechanical Properties of Hydraulic Concrete*, China Three Gorges University, Yichang, 2018.

[14] American Concrete Institute, *Specification for Hot Weather Concreting (ACI 305.1-06)*, American Concrete Institute, Michigan USA, 2007.

[15] Q. Li, Q. C. Wang, and R. L. Zhang, "Analysis of crack resistance, mechanical properties and pore size distribution of concrete in a certain environment of dryness-coldness and large range of temperature," *Bulletin of the Chinese Ceramic Society*, vol. 36, no. 9, pp. 2880–2885, 2017.

[16] Y. Tang and J. Guo, "Analysis of factors affecting the strength of ordinary concrete," *Sichuan Building Materials*, vol. 46, no. 10, pp. 6-7, 2020.

[17] F. Collins and J. G. Sanjayan, "Effect of pore size distribution on drying shrinking of alkali-activated slag concrete," *Cement and Concrete Research*, vol. 30, no. 9, pp. 1401–1406, 2000.

[18] T. M. Wang, *Control of Cracking in Engineering Structure-Principle of "Reist and Release" for Alternative Bay Construction Method Cracking Control of Super Long Mass Concrete (in Chinese)*, China Building Industry Press, Beijing China, 2007.

[19] X. G. Wang, *Practical Calculation Method for Mass Concrete Temperature Stress of and Crack Control Engineering Example*, People's Communications Publishing House Co., LTD., Beijing China, 2017.

[20] Z. H. Wang, S. P. Yu, Y. Liu, and Y. Z. Liu, "The impact of temperature difference between day and night on thin-walled concrete structure," *Applied Mechanics and Materials*, vol. 212-213, pp. 970–973, 2012.

[21] G. Bai, "Causes and control of concrete cracks in building construction," *Cheng Shi Jianshe LiLun Yan Jiu*, vol. 28, pp. 117–148, 2017.

[22] D. C. Ma, "Discussion on the pouring technology of mass concrete in equatorial region under sea environment," *Construction & Design for Engineering*, vol. 69, no. 11, pp. 188–190, 2021.

[23] A. B. Recov, *Theory of Heat Transfer (in Chinese)*, L. J. Qiu, Ed., Higher Education Press, Beijing China, 1995.

[24] R. Springenschmid, R. Breitenbucher, and M. Mangold, "Development of the cracking frame and the temperature-stress testing machine," in *Thermal Cracking in Concrete at Early Ages*, pp. 137–144, CRC Press, 1994.

[25] J. D. Xin, Y. Liu, G. X. Zhang et al., "Evaluation of early-age thermal cracking resistance of high w/b, high volume fly ash (HVFA) concrete using temperature stress testing machine," *Case Studies in Construction Materials*, vol. 16, article e00825, 2022.

[26] J. L. Sun, *Thermal-Mechanical Analysis and Crack Research of Mass Concrete Bearing Platform*, Shandong University, Jinan, 2015.

[27] Z. T. Yang, *Simulation Study of Temperature Control and Anticracking in Mass Concrete Pile Cap*, Harbin Institute of Technology, Harbin, 2010.

[28] C. Yang, *Monitoring and Analysis of Temperature Stress of Mass Concrete in the Foundation of Shaking Table Array*, Beijing University of Civil Engineering and Architecture, Beijing, 2020.

[29] X. S. Wang, *Study on Anti-Crack and Temperature Stress of Raft Foundation Considering the Function of Rebar in Construction Period*, Chang'an University, Xi'an, China, 2015.

[30] J. X. Huang, *Design and Construction about Planceer of Mass Concrete in Basement*, South China University of Technology, Guangzhou, 2011.

[31] Z. X. You, *Research on Temperature Fields and Stress Fields and Temperature Control Measures of Mass Concrete*, Chongqing University, Chongqing, 2018.

[32] R. Z. Li and R. Y. Li, "Crack analysis of hollow block based on ABAQUS," *Water Resources Planning and Design*, vol. 31, no. 12, pp. 199–202, 2018.

[33] S. T. Lin, X. L. Zhong, X. C. Peng et al., *Standard for Construction of Mass Concrete GB50496-2018*, MCC, Beijing China, 2018.

[34] Q. L. Ma, *Test Method on Tensile Creep of Cement_Based Materials at Ultra-Early Age*, Yan Shan University, Qinhuangdao, 2020.

[35] Z. J. Li, Z. H. Li, P. Yu, L. C. Xu, and X. D. Fu, "Monitoring and finite element analysis of temperature and stress field of mass concrete for tower platform," *Journal of Railway Science and Engineering*, vol. 17, no. 11, pp. 2892–2900, 2020.

[36] Z. C. Sun, *Research on Safety of Deepwater Pile Foundation Construction Platform in Reservoir Area*, Chongqing Jiaotong University, Chongqing, 2018.

[37] J. H. Liu, "Crack risk analysis and control countermeasures of Y pier of long-span continuous rigid frame bridge," *Construction & Design for Engineering*, vol. 67, no. 11, pp. 114–117, 2019.

[38] W. Y. Chen and Y. H. Chen, "The finite element analysis of a mass concrete foundation slab jump silo method in Kunming," *Low Carbon World*, vol. 11, no. 5, pp. 156-157, 2021.

[39] Y. Lü, *Study on Crack Resistance of High Strength Fly Ash Concrete under the Condition of Equal Strength*, Ningxia University, Ningxia, 2020.

[40] M. G. Yang, "Fire stability analysis of high fire wall based on limit analysis," *Proceedings of The 30th National Conference on Structural Engineering*, vol. 1, pp. 379–388, 2020.

[41] G. C. Liao, Z. Y. Wu, B. Wang, and D. S. Guan, "Field monitoring of hydration temperature and bearing capacity of cast-in-place pile in thick silt stratum," *Guangdong Architecture Civil Engineering*, vol. 28, no. 11, pp. 79–83, 2021.

[42] H. T. Li, "Numerical simulation on crack-free construction of super large area concrete ground structure," *Chongqing Architecture*, vol. 14, no. 6, pp. 43–47, 2015.

[43] Q. Zhang, Y. F. Li, and X. L. Gong, "Ground temperature prediction based on shallow-surface ground temperature and in-situ thermophysical parameters," *Geological Bulletin of China*, vol. 40, no. 10, pp. 1713–1719, 2021.

[44] H. P. Hu, S. X. Yang, and Z. D. Lei, "A numerical simulation for heat and moisture transfer during soil freezing," *Journal of Hydraulic Engineering*, vol. 37, no. 7, pp. 1–8, 1992.

[45] American Concrete Institute, *Specification for Hot Weather Concreting (ACI 308-01)*, American Concrete Institute, Michigan USA, 2001.

[46] Q. Gao, Z. Wen, F. Ming, J. Liu, M. Zhang, and Y. Wei, "Applicability evaluation of cast-in-place bored pile in permafrost regions based on a temperature-tracking concrete hydration model," *Applied Thermal Engineering*, vol. 149, pp. 484–491, 2019.

[47] G. M. Moelich, J. E. van Zyl, N. Rabie, and R. Combrinck, "The influence of solar radiation on plastic shrinkage cracking in concrete," *Cement and Concrete Composites*, vol. 123, article 104182, 2021.